Title

Comparing time-dependent density functional theory with many-body perturbation theory for semiconductors: Screened range-separated hybrids and the GW plus Bethe-Salpeter approach

Journal

Physical Review Materials, 3(6)

ISSN

2476-0455

Authors

Wing, Dahvyd
Haber, Jonah B
Noff, Roy
et al.

Publication Date

2019-06-01

DOI

10.1103/physrevmaterials.3.064603

Comparing Time-Dependent Density Functional Theory with Many-Body Perturbation Theory for Semiconductors: Screened Range Separated Hybrids and the GW plus Bethe-Salpeter Approach

Dahvyd Wing,[1] Jonah B. Haber,[2,3] Roy Noff,[1] Bradford Barker,[2,3] David A. Egger,[4] Ashwin Ramasubramaniam,[5] Steven G. Louie,[2,3] Jeffrey B. Neaton,[2,3,6,7] and Leeor Kronik[1]

[1]*Department of Materials and Interfaces, Weizmann Institute of Science, Rehovoth 76100, Israel*
[2]*Department of Physics, University of California, Berkeley, Berkeley, California 94720, USA*
[3]*Materials Sciences Division, Lawrence Berkeley National Laboratory, Berkeley, California 94720, USA*
[4]*Institute of Theoretical Physics, University of Regensburg, Regensburg, 93053, Germany*
[5]*Department of Mechanical and Industrial Engineering, University of Massachusetts Amherst, Massachusetts, 01003, USA*
[6]*Molecular Foundry, Lawrence Berkeley National Laboratory, Berkeley, CA 94720, USA*
[7]*Kavli Energy NanoSciences Institute at Berkeley, Berkeley, CA, 94720, USA*

(Dated: April 15, 2019)

We present band structure and optical absorption spectra obtained from density functional theory (DFT) and linear response time-dependent DFT (TDDFT) calculations using a screened range-separated hybrid (SRSH) functional, including spin-orbit coupling, for seven prototypical semiconductors. The results are compared to those obtained from highly converged many-body perturbation theory calculations using the GW approximation and the GW plus Bethe-Salpeter equation (GW-BSE) approaches. We use a single empirical parameter for our SRSH calculations, fit such that the SRSH band gap reproduces the GW band gap at the Γ point. We then find that ground-state generalized Kohn-Sham SRSH eigenvalues accurately reproduce the band structure obtained from GW calculations, typically to within 0.1-0.2 eV, and optical absorption spectra obtained using TDDFT with the SRSH functional agree well with those of GW-BSE, with a mean deviation of 0.03 eV and 0.11 eV for the location of the first and second absorption peaks, respectively, at a fraction of the computational cost.

I. INTRODUCTION

Many-body perturbation theory, using the GW approximation[1–5] and the Bethe-Salpeter equation (BSE),[6–9] has become a standard approach for calculating accurate optical spectra of solid state materials. In principle, time-dependent density functional theory (TDDFT)[10–13] can also provide accurate optical absorption spectra, potentially at a lower cost.[9] However common TDDFT approximations, such as the adiabatic local density approximation (ALDA), fail when calculating the optical absorption of semiconductors,[14,15] i.e., the line shape is shifted and distorted and in particular excitonic effects are not captured. Therefore, TDDFT methods that are accurate yet inexpensive for solid state materials is an ongoing challenge.[9,11,16–19]

There are two main challenges that TDDFT methods need to address in order to predict accurate optical spectra of semiconductors. One is that Kohn-Sham (KS) eigenvalues underestimate the fundamental band gap.[20,21] While an exact TDDFT method would be able to compensate for the underestimated fundamental gap, a TDDFT method using the adiabatic approximation is unable to compensate for it.[11] Thus common TDDFT spectra are red shifted with respect to experiment.[14] The second challenge is that the exchange-correlation kernel, $f_{xc}(q+G, q+G')$ (where G and G' are reciprocal lattice vectors and q is a reciprocal-space vector in the Brillouin zone), must accurately capture the necessary $\frac{1}{q^2}$ behavior in the long wavelength limit, i.e. $G = G' = 0$ and $q \to 0$, in order to accurately describe excitonic effects.[15,22,23] Unfortunately, this is not satisfied by self-consistently derived semilocal exchange-correlation kernels, i.e., those obtained by taking the functional derivative of the exchange-correlation potential with respect to the density.

Several solutions to these difficulties have been proposed. For example, the so-called nanoquanta kernel is constructed from the BSE kernel, though this inevitably makes it as expensive as BSE.[22] Long range corrected kernels have been proposed, which approximate the kernel as $\frac{\alpha}{q^2}$ (or some variation of this form), where α is a parameter to be set.[18,24] The bootstrap method iteratively builds the kernel using the random-phase approximation (RPA) for the dielectric function until self-consistency is reached.[17,25] Another proposed method involves a kernel based on the dielectric function of the jellium with a gap model (JGM).[19,26] Methods using a meta-GGA self-consistently derived kernel have also been proposed.[27] Finally, methods have been proposed which use self-consistently derived kernels from hybrid functionals in the generalized Kohn-Sham framework.[16,28–30]

In all but the hybrid functional approaches, the band gap problem is handled separately from the issue of developing a kernel with a $\frac{1}{q^2}$ dependence. Usually the fundamental band gap is corrected via a scissor shift or by GW calculations. In hybrid functionals these two issues can be dealt with simultaneously without the need for corrections from methods beyond DFT. The

formalism remains fully within DFT/TDDFT, because hybrid functionals are within the generalized Kohn-Sham scheme.[31,32] In particular, screened range-separated hybrid (SRSH) functionals were specifically developed to demonstrate the ability of hybrid functionals to solve both issues simultaneously.[30] SRSH functionals accomplish this by taking advantage of the degrees of freedom afforded by their functional form, which varies the fraction of exact exchange used based on the distance between the interacting electrons.

From a formal perspective, Kohn-Sham DFT produces incorrect band gaps even in principle owing to the derivative discontinuity, i.e., a uniform "jump" in the exchange-correlation potential across an integer number of electrons.[20,21,33,34] SRSH functionals can in principle overcome this limitation as they arise from generalized Kohn-Sham theory, where an appropriately chosen nonlocal potential operator can strongly reduce the derivative discontinuity.[31,35–37] The optimal choice of the nonlocal potential, however, may be system dependent.[35] Thus, when one parameter controlling the fraction of exact exchange included in the SRSH functional is fit so that the functional reproduces the fundamental band gap of a GW calculation, as was done in Ref 30, this indirectly reduces the derivative discontinuity. Notably, in that work, fitting for the fundamental band gap greatly improved the agreement between SRSH eigenvalues and GW quasiparticle energies across the entire band structure, including locations in the Brillouin zone far away from the band gap minimum.

SRSH functionals include the correct $1/q^2$ behavior in the kernel by using screened exact exchange for large distances, r, and thus have the correct asymptotic $\frac{1}{\epsilon_\infty r}$ behavior, where ϵ_∞ is the high-frequency (electronic response only) dielectric constant. This leads to the exchange-correlation kernel having the correct $\frac{1}{q^2}$ behavior.[16,30]

From a pragmatic point of view, the flexibility of SRSH's functional form to match the GW band structure allows one to investigate how well TDDFT using a kernel derived from a hybrid functional can approximate GW-BSE results. In Ref. 30, time-dependent SRSH (TD-SRSH) and GW-BSE were compared for silicon and lithium fluoride, with promising results. Here we compare SRSH to GW and TD-SRSH to GW-BSE for a broader class of seven prototypical semiconductors, including spin-orbit coupling effects. We find excellent agreement between SRSH and GW for bands close to the band edges and excellent agreement between TD-SRSH and GW-BSE optical absorption spectra.

II. METHODOLOGY

A. Benchmark systems

In this work, we study seven prototypical semiconductors: Si, AlP, AlAs, AlSb, GaP, GaAs, and InP. The materials investigated are selected from an extensively used benchmark of semiconductors[38,39] because they allow us to compare our one-shot G_0W_0 results to previous calculations,[40] and because these semiconductors do not suffer from severe starting point issues that require special attention in the GW approximation, notably the spurious metallic state predicted by semi-local DFT calculations for small band gap semiconductors. Experimental room-temperature lattice parameters are used for all calculations, see Table I.

B. Many-body perturbation theory calculations

Our many-body perturbation theory calculations proceed from a DFT starting point computed within the Perdew-Burke-Ernzerhof (PBE) semi-local approximation for the exchange-correlation functional.[41] Our DFT starting point calculations are performed using the Quantum Espresso[42,43] plane-wave code and employ fully relativistic optimized norm-conserving (NC) Vanderbilt pseudopotentials[44] obtained from the online repository, pseudo-dojo. For Ga, In, and Sb, we include one complete shell of semicore states as valence. This is known to be important for correctly describing the electronic structure.[45] For all materials considered, DFT ground state densities are computed on a shifted $8 \times 8 \times 8$ Monkhorst-Pack k-grid, centered around the (½ ½ ½) point. A kinetic energy cutoff of 200 Ry is used for materials containing either Ga or In; for all other materials the cutoff is set to 100 Ry. Calculations include spin-orbit coupling for all materials except Si and AlP, where it is negligible.

Kohn-Sham (KS) states obtained from the aforementioned calculation are subsequently used to perform a fully relativistic, full-frequency, one-shot G_0W_0 calculation of the electronic self-energy operator, $\Sigma = iGW$[4] using the BerkeleyGW package.[46] Here, G denotes the single particle Green's function and W the dynamically screened Coulomb interaction. The irreducible polarizability, χ, is computed within the random phase approximation and related to W through the inverse dielectric function ϵ^{-1} in the usual manner, namely, $\epsilon = 1 - v\chi$ and $W = \epsilon^{-1}v$, where v is the bare Coulomb interaction. By fully relativistic, we mean to indicate that G is constructed using the two component (spinor) KS states computed at the DFT level.[47–51] This is to be contrasted with prior GW calculations where G was computed with the scalar KS states and the effects of spin-orbit coupling were included perturbatively.[52] Additionally, in this work, we explicitly compute the full-frequency (FF) dielectric tensor, $\chi_{G,G'}(q,\omega)$, as opposed to using a plasmon-pole model.[4,53] For the FF convolution of G with W, we use the standard contour-deformation technique[54,55] and evaluate $\chi_{G,G'}(q,\omega)$ at 15 frequencies along the imaginary axis. To further reduce the substantial computational cost of computing the FF dielectric tensor, we use the static subspace approxima-

tion. In this approximation, a low-rank decomposition of the static polarizability, $\chi_{G,G'}(q,0)$, is performed, obtaining the largest 40 eigenvectors. These eigenvectors are subsequently used as a basis for expanding the FF polarizability, $\chi_{G,G'}(q,\omega)$. The above procedure greatly reduces the overall cost of the FF calculation while still maintaining a high level of accuracy. A detailed description of this and similar methods can be found in Refs. 56–60. The dielectric cutoff and the number of empty states used in our computation of χ and Σ are detailed in Table I. These values are chosen based on previous calculations carried out by Malone and Cohen.[40] These values and our other choices for convergence are estimated to converge the quasiparticle gap to within 10 meV.

Finally, excitonic wavefunctions and energies are computed by solving the Bethe-Salpeter equation for the electron-hole correlation function in the basis of Kohn-Sham states.[7,8] A detailed discussion of the equations solved and their relation to response properties can be found in, e.g., Refs. 9, 46, and 61. Here, for the electron-hole kernel, we use the approximation $K_{eh} = \frac{\delta V_H}{\delta G} + \frac{\delta \Sigma}{\delta G} \approx -W_d(\omega = 0) + V_x$, where V_H is the Hartree potential, $W_d(\omega = 0)$ denotes the statically screened direct operator, and V_x is the Coulomb exchange operator. We make the Tamm-Dancoff approximation[9] when constructing the electron-hole kernel, and we expand K_{eh} in a set of 4 valence and 3 conduction bands for Si, 3 valence and 3 conduction bands for AlP, and 6 valence and 6 conduction states for all other compounds. Finally, to obtain converged exciton properties K_{eh} is interpolated from an $8 \times 8 \times 8$ to a $14 \times 14 \times 14$ k-grid shifted by (0.1, 0.45, 0.75). Further details on the convergence of these calculations with respect to number of bands used and k-point sampling can be found in the supplementary material (SM).

C. DFT - SRSH Calculations

1. General

In the SRSH functional,[62] the exchange part of the Coulomb interaction is partitioned using the identity

$$\frac{1}{r} = \frac{\alpha + \beta \operatorname{erf}(\gamma r)}{r} + \frac{1 - [\alpha + \beta \operatorname{erf}(\gamma r)]}{r}, \qquad (1)$$

with exchange owing to the first term treated by a Fock-like operator and exchange owing to the second term treated by semi-local exchange, in our case based on the PBE functional. The full form of the SRSH exchange-correlation functional can then be expressed as:

$$E_{xc}^{\mathrm{SRSH}} = (1-\alpha)E_{KSx}^{SR} + \alpha E_{xx}^{SR} + [1-(\alpha+\beta)]E_{KSx}^{LR} + (\alpha+\beta)E_{xx}^{LR} + E_{KSc}, \qquad (2)$$

where the subscripts KSx and KSc denote (semi)local KS exchange and correlation, respectively, and xx is exact (Fock) exchange. Exchange is partitioned into short range (SR) and long range (LR) components that are scaled by the error function such that there is seamless transition between the two regimes. α, β, and γ are parameters. α controls the fraction of short range exchange and in this work it is set to 0.25 throughout, as in the PBE0 global hybrid functional. This choice is not unique, however (see the SM). In line with previous work,[30] we set $\alpha+\beta = \frac{1}{\epsilon_\infty}$, where ϵ_∞ is the high-frequency dielectric constant. This constraint on β ensures that the SRSH functional has the correct $\frac{1}{\epsilon_\infty r}$ asymptotic behavior. In this work, the range-separation parameter, γ, is fit to obtain the direct fundamental band gap at Γ as calculated by GW, in the absence of spin-orbit coupling for either approach. *A priori* selection of the parameters of the SRSH functional is an ongoing challenge.[62–65] Our parameter choice removes differences due to band gaps so that TD-SRSH and GW-BSE can be directly compared.

We use the Vienna *ab initio* simulation package (VASP), a plane-wave code,[66] using PBE-based projector-augmented waves (PAWs) for treating core electrons, to perform SRSH functional calculations.[67] For gallium and indium the PAWs include semi-core d-states. PBE eigenvalues calculated using VASP are found to agree to within ∼20 meV with the eigenvalues of the starting point calculations for GW using Quantum Espresso with norm-conserving pseudopotentials. This ensures that significant differences between SRSH and many-body perturbation theory calculations, if any, do not arise from the different treatment of core electrons.

2. Dielectric response

The ion-clamped, high-frequency dielectric constant, ϵ_∞, is calculated from the change in polarization in response to a finite electric field[68,69] using VASP. The Heyd-Scuseria-Ernzerhof (HSE)[70] short-range hybrid functional is used for this calculation, as it has been shown to lead to relatively accurate dielectric constants.[28] Due to the fact that the semiconductors in this study have large dielectric constants, SRSH band structures and optical spectra of semiconductors are not strongly affected by the exact value of the dielectric constant, as long as the SRSH functional is fitted so that the fundamental band gap is matched to that of GW (see SM). Thus the choice of which functional to use to calculate the dielectric constant is of little consequence. In these calculations local field effects are included for both Hartree and exchange-correlation potentials, and spin-orbit coupling is included for all materials except Si and AlP. The plane wave cutoff is 300 eV for all materials. An 11×11×11 Monkhorst-Pack k-grid is used, converging the dielectric constant to within 0.1 for PBE calculations. Dielectric constants are reported in Table I.

3. Band gap and band structure

For fitting the SRSH gap to that obtained from GW and calculating the band structure, an $8 \times 8 \times 8$ Monkhorst-Pack k-grid is used with a 300 eV plane wave energy cutoff. With these parameters, the total energy is converged to ∼3 meV/atom and the SRSH KS band gap to ∼15 meV. The fitted values for the range-separated parameter are presented in Table I. The WANNIER90 software package[71] is then used to obtain band structures.

4. TD-SRSH

TDDFT linear response calculations are performed by solving the Casida equations[74] within the Tamm-Dancoff approximation.[12,75] For a detailed discussion of the equations in the TD-SRSH case, see Refs. 30 and 61. The exchange-correlation kernel, f_{xc}, is evaluated using 3 valence bands and 4 conduction bands for AlP, 4 valence bands and 4 conduction bands for Si, and 6 valence bands and 6 conduction bands for all other materials. In addition, an energy window of 15 eV is used to reduce the number of poles considered. The energy plane wave cutoff is set to 200 eV for Si, AlP, AlAs, and AlSb, 230 eV for GaP and GaAs, and 210 eV for InP. Increasing all these parameters affected the imaginary part of the dielectric function by less than 0.3% at the first few absorption peaks.

The k-grid used is a shifted $14 \times 14 \times 14$ Monkhorst-Pack grid. Convergence of the TDDFT and BSE optical spectra is greatly facilitated by a judicious choice of a grid shift that attempts to evenly sample the different regions of the Brillouin zone that contribute to the optical transitions. As all semiconductors studied here are zinc-blende structures, their Brillouin zones and band structures are very similar and thus we expect that a single shift for all of them suffices. We therefore employ the following heuristic approach: For each of the 7 materials considered here, we generate 20^3 uniform $10 \times 10 \times 10$ k-grids, each shifted by a different amount, $\frac{n}{20}b_1 + \frac{m}{20}b_2 + \frac{l}{20}b_3$, where b_1, b_2, and b_3 are the reciprocal lattice vectors; and n,m, and l are integers between 0-19 (in practice, we use symmetry to reduce the number of generated k-grids to 447). A DFT calculation at the PBE level is performed using each k-grid. We then compute a figure of merit for each k-grid as follows. Let $\{E_i\}$ be the ordered set from least to greatest value of the direct KS band gap at each k-point, i, in a single DFT calculation, $E_i = \epsilon_{\mathrm{CBM},i} - \epsilon_{\mathrm{VBM},i}$. Then, define the average spacing in energy between E_i's as $\overline{\Delta E} = (E_{N_k} - E_1)/N_k$, where N_k is the number of k-points for the k-grid. We may then calculate the variance of the spacing in energy between band gaps in the ordered set as

$$\sigma^2 = \frac{1}{N_k}\sum_{i-1}(E_{i+1} - E_i - \overline{\Delta E})^2 \qquad (3)$$

We select the k-shift leading to the smallest variance for all the materials calculated, which is found to be (0.1, 0.45, 0.75). We estimate that with this approach peak positions are converged to ∼0.2 eV and peak heights to ∼10%; see the SM for further discussion of convergence. A Gaussian broadening of 0.1 eV is used. With this choice, computed absorption peaks have the same width as room-temperature experimental ones.

III. RESULTS AND DISCUSSION

A. GW band gaps and band structures

Because we use many-body perturbation theory as a benchmark of our SRSH results, we begin by assessing how the present GW calculations compare with prior work. A summary of GW- and SRSH-computed direct and indirect band gaps is given in Table II. The indirect band gaps are obtained from the Wannier-interpolated band structure, as the conduction band minimum does not lie exactly at the X point. Our GW calculations are very similar to those of Malone and Cohen[40] in that we use the same overall approach, the same computational software, and strive for a similar level of tight convergence. Our calculations differ from Ref. 40, however, in some details: we use a PBE starting point (as opposed to LDA), an FF treatment of the dielectric tensor (in contrast to the generalized plasmon-pole model), and a fully relativistic treatment of spin-orbit coupling (instead of a perturbative treatment). We also include semicore states in the Sb pseudopotential, and increase the k-point sampling for Ga and In compounds. Despite these differences, with the exception of GaAs (elaborated on below), we find our GW band structures to be in good agreement with those of Ref. 40, especially for Si, AlP, and AlAs.

For AlSb, we find a GW direct band gap which is roughly 0.2 eV larger than that predicted in Ref. 40, which we attribute to the semicore states we include in the Sb pseudopotential. At the PBE level, we observe that the fundamental band gap for AlSb, without spin-orbit coupling, increases by 0.11 eV when one treats the Sb $4s4p$ states, in addition to the $4d5s5p$ states, as valence in the pseudopotential. For InP and GaP, we find that our GW band gaps throughout the BZ are slightly smaller (∼ 0.2 eV) than those reported in Ref. 40, despite the fact that the PBE gaps for these compounds are roughly 0.2 eV larger than the LDA gaps. We attribute the majority of this discrepancy to different treatment of the frequency dependence of the dielectric function. Indeed, previous studies suggest that plasmon-pole models can somewhat overestimate gaps when compared with numerical integration schemes.[77]

Next, we compare GW band gaps to experimental optical gaps, which is reasonable because the exciton binding energies for these materials are small.[72,78] We find that GW indirect band gaps are within 0.2 eV of

	a_{lat} ($\mathring{A}$)	χ_{cut} (Ry)	χ_{bands}	Σ_{bands}	$\epsilon_\infty^{\text{theory}}$	$\epsilon_\infty^{\text{expt}}$	γ ($\mathring{A}^{-1}$)
Si	5.43	25	300	500	11.3	11.97	0.62
AlP	5.46	28	500	600	7.3	7.5	0.80
AlAs	5.66	30	1000	1200	8.2	8.2	1.25
AlSb	6.14	23	1000	1400	9.8	10.24	0.63
GaP	5.45	64	1000	2000	8.9	9.11	1.15
GaAs	5.65	65	1200	2400	10.5	10.86	2.5
InP	5.87	35	800	2000	8.9	9.52[a]- 10.9	1.3

TABLE I. Room temperature experimental lattice parameters[72] used for both our GW and SRSH calculations (left side), convergence parameters for GW (middle section), and functional parameters for SRSH (right side). χ_{cut} is the plane wave energy cutoff for evaluating the irreducible polarizablity; χ_{bands} and Σ_{bands} are the number of bands used to evaluate the irreducible polarizability and the self-energy operator, respectively. $\epsilon_\infty^{\text{theory}}$ is the ion-clamped dielectric constant using HSE; $\epsilon_\infty^{\text{expt}}$ is the experimental high-frequency dielectric constant at room-temperature (from Ref. 72, (a) from Ref. 73). In the far right column, we provide the range-separation parameter (γ in Eq. 1) for which the SRSH direct band gap matches the GW direct band gap

	$E_{g,\text{direct, fund}}$ (eV)		$E_{g,\text{direct, opt}}$ (eV)
	SRSH (no-SOC/SOC)	GW (no-SOC/SOC)	Expt.
Si	3.24	3.25	3.35[a]
AlP	4.26	4.25	3.63
AlAs	2.82/2.71	2.79/2.69	3.03
AlSb	2.32/2.12	2.32/2.10	2.30
GaP	2.60/2.57	2.62/2.59	2.79
GaAs	1.07/0.95	1.07/0.95	1.42
InP	1.31/1.28	1.34/1.30	1.34
	$E_{g,\text{indirect, fund}}$ (eV)		$E_{g,\text{indirect, opt}}$ (eV)
Si	1.11	1.20	1.12
AlP	2.39	2.50	2.45
AlAs	2.09/1.99	2.08/1.98	2.15
AlSb	1.80/1.55	1.77/1.55	1.62
GaP	2.22/2.17	2.33/2.30	2.27

TABLE II. SRSH and GW fundamental band gaps with and without spin-orbit coupling. As mentioned in the text, all GW calculations are one-shot from a PBE starting point. Owing to very small exciton binding energies in these materials, these can be compared to experimental optical band gaps. All experimental data is at 300K and taken from Ref. 72 except for a) which is at 80K from Ref. 76.

the indirect experimental optical gaps. The agreement between GW and experimental direct band gaps is not as good, which could be due to the fact that the assignment of the direct optical band gap for indirect semiconductors is experimentally challenging. In particular, for AlP we find that the commonly reported experimental direct band gap (3.63 eV) differs substantially from the GW gap (4.25 eV). However, our direct band gap is in agreement with previous GW results.[39,40] Furthermore, Zhu et al.[39] questioned the experimental assignment of the 3.63 eV feature to the direct band gap,[78,79] suggesting that it is most likely the 3.56 eV Γ_{15v} to X_{3c} indirect transition. As shown below, both BSE and TDDFT computed optical spectra of AlP are in close agreement with the experimental optical spectrum, lending further credence to this result.

Lastly, for GaAs, we find a direct gap of 0.95 eV, which is 0.36 eV lower than what was reported in Ref. 40 and about 0.5 eV lower than experiment. Further testing indicates that the PBE starting point, denser k-grid, FF treatment of the dielectric, and inclusion of spin-orbit coupling all tend to close the gap at Γ relative to Ref. 40 (see the SM). This result is somewhat reduced relative to initial GW calculations for GaAs that were in much better agreement with experiment,[4,45] but is consistent with recent calculations. For example, Klimeš et al.[80] reported a one-shot G_0W_0 gap of 1.23 eV using a PBE starting point. They suggested that contributions from localized Ga 3d states in the Coulomb hole term may be responsible for the reduced gap relative to experiment. The use of methods beyond one-shot G_0W_0 may address this issue, including quasiparticle self-consistent GW,[81] or starting from hybrid or static-COHSEX wave functions.[82] Furthermore, in future work, we plan to explore using a hybrid functional starting point.[83–85] Regardless of the discrepancy between G_0W_0 and experiment for GaAs, the fact that the GW results are well converged makes them suitable for our purposes because the SRSH functional is fit to the GW calculations and then TD-SRSH calculations are primarily compared to GW-BSE calculations, rather than to experiment.

B. SRSH band gaps and band structures

Comparing SRSH to GW, we first point out that while SRSH is only fit to the GW direct band gap, the SRSH and GW indirect band gaps also agree to within 0.11 eV. Furthermore, SRSH is fit to GW without spin-orbit coupling and continues to exhibit good agreement after spin-orbit coupling is independently taken into account in both approaches. A comparison of SRSH and GW band structures for all seven semiconductors is given

in Figure 1. Very good agreement between SRSH and GW band structures near the band edges is obtained throughout. Quantitatively, the mean absolute deviation for the top two valence bands and bottom two conduction bands (four valence bands and four conduction bands accounting for using spin-orbit coupling) is 0.06 ± 0.05 eV, with the largest deviation being 0.35 eV. There are larger differences for lower lying valence bands and higher conduction bands. This, however, is to be expected, given that SRSH can be viewed as a static approximation to the self-energy, which is known to produce larger deviations away from band edges.[36,86] Additionally, GW can underbind low-lying bands, especially when those bands derive from states with localized d-character[87]. We also note that, in any case, neither SRSH nor GW calculations fully include electron-plasmon coupling, which may become important in this energy regime and modify the structure of the lowest bands.[88]

To further assess the ability of SRSH to capture quasiparticle (QP) corrections, in Figure 2 we plot corrections to DFT-PBE eigenvalues, $\varepsilon_{QP} - \varepsilon_{PBE}$, as a function of the DFT-PBE eigenvalues, ε_{PBE}, for silicon. Silicon exhibits the largest differences between SRSH and GW eigenvalues. We also include static-COHSEX eigenvalues for comparison. For clarity, in all cases we rigidly shift the corrections so that the valence band maximum for the PBE, SRSH, GW, and static-COHSEX calculations all align. We plot the three highest valence bands and four lowest conduction bands. We first note that the FF-GW correction narrows the bandwidth, relative to PBE, for lower valence bands. This is consistent with previous GW calculations using a generalized plasmon pole model, but is more pronounced and occurs at energies closer to the band edges.[40] SRSH nearly linearly widens the valence bandwidth and conduction bandwidth with a slope similar to the static-COHSEX approximation. This is in line with the interpretation of SRSH as a static approximation of the self-energy. We also note that the small difference between the SRSH and FF-GW conduction band minima stems from the fact that we fit the SRSH functional to match the direct band gap, not the indirect band gap.

C. GW-BSE and TD-SRSH optical spectra

We now turn to the comparison of TD-SRSH and BSE calculations of optical absorption spectra, focusing especially on low-lying excitonic states. We emphasize that no further fitting takes place at the TDDFT level. Once the exchange-correlation functional is fixed, the exchange-correlation potential and kernel are self-consistently derived from it via first and second functional derivatives, respectively. In Figure 3 we show the optical absorption spectrum of TD-SRSH, BSE, and experiment. Where possible, we include both room-temperature and low temperature experimental data. Despite the absence of full convergence with respect to the k-grid (see section II C 4 and the SM), SRSH and BSE predict peak locations and line shapes in close agreement with each other and with experimental values. Quantitatively, the mean absolute deviation between TD-SRSH and BSE of the absorption peak position is 0.03 eV for the E_1 peak and 0.11 eV for the E_2 absorption peak. It is noteworthy that both calculations correctly describe the spin-orbit coupling-split E_1 peaks of AlSb.[89]

Further evidence for the success of the TD-SRSH method is that in the cases where BSE differs from experiment, TD-SRSH follows suit. This can be seen for the red-shift of the E_1 peak (the "first" peak) for AlAs, GaP, and GaAs; the lack of spin-orbit coupling split E_1 peaks for GaAs; and the overestimation of oscillator strengths for the E_2 peak of AlSb, GaP, and GaAs. It is likely that the red-shift is the result of the slight underestimation of the direct band gap for these materials by GW. Additionally, BSE and TD-SRSH show similar spurious peaks at the onset of absorption for the GaP, GaAs, and InP. This is likely due to lack of complete k-point convergence and denser k-grids would likely smooth the onsets of absorption (see the SM).

As for the differences between the TD-SRSH and BSE calculations, we find that E_1 oscillator strengths predicted by BSE are closer to those of the low temperature experimental data than those predicted by SRSH. Since we neglect temperature effects in our calculations, apart from using room-temperature lattice parameters, this provides a more relevant comparison. Generally, the oscillator strengths of the SRSH spectra at lower energy are reduced relative to those of GW-BSE and experiment, possibly indicating an underestimate of the electron-hole interaction.

We attribute TD-SRSH's success in reproducing BSE results to several reasons. First, the low-lying excitations considered here are composed primarily of electron-hole pairs near the band edges, and we have seen in these materials that SRSH describes the GW quasiparticle energies in this range well. Second, in these materials, the exciton binding energy is much smaller than the plasmon frequency and we thus expect dynamical screening to be of limited importance for low energy spectral features. This is ideal for SRSH because it is inherently a static approximation. Indeed, the importance of dynamical screening has been investigated in early BSE calculations and it has become common practice to take into account only the static dielectric tensor when constructing the BSE kernel.[8] Finally, SRSH captures important exchange-correlation effects via the $\frac{1}{q^2}$ behavior in the kernel.[15,22,23,30]

IV. CONCLUSION

In conclusion, we have shown that, with one material-specific fitting parameter, the SRSH functional yields band structures in close agreement with GW and optical spectra in close agreement with BSE and experimental

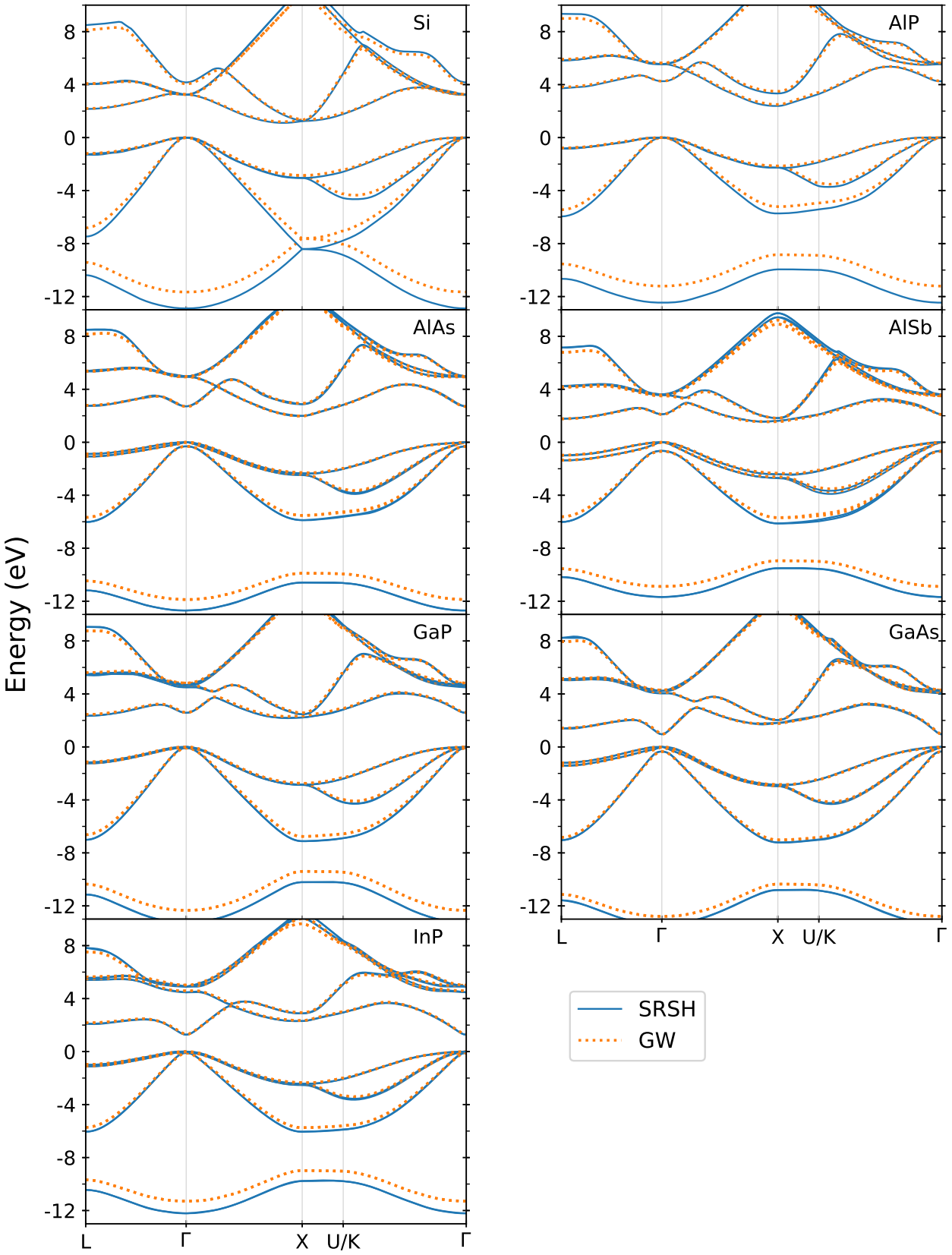

FIG. 1. Band structures of semiconductors studied in this work: SRSH (with the range-separation parameter chosen to fit the direct GW band gap) - blue solid lines, GW - orange dotted lines. All calculations include spin-orbit coupling, except for Si and AlP.

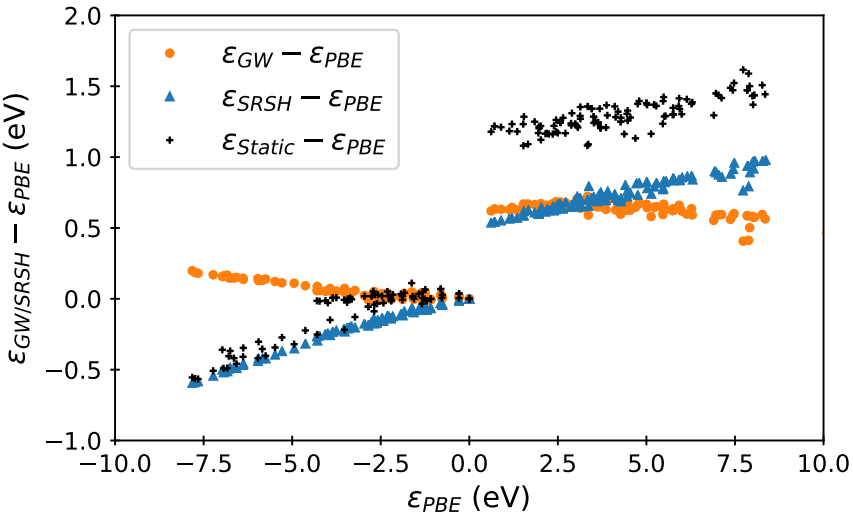

FIG. 2. Differences between PBE eigenvalues and full-frequency GW (orange circles), SRSH (blue triangles), and static COHSEX eigenvalues (black crosses) for silicon, as a function of the PBE eigenvalue. Each eigenvalue spectrum is normalized independently so that the valence band maximum is at 0 eV.

data, for a range of semiconductors. This shows that TDDFT using range-separated kernels derived from exact exchange can be on par with GW-BSE calculations. Thus, SRSH can be used for semiconductor systems where GW calculations may be too expensive, as long as the band gap is known.

This work was primarily supported via a US-Israel National Science Foundation - Binational Science Foundation (NSF-BSF) grant, DMR-1708892. Partial support from the Theory Program at the Lawrence Berkeley National Laboratory through the Office of Basic Energy Sciences, U.S. Department of Energy, under Contract No. DE-AC02-05CH11231, was also provided. DAE acknowledged funding provided by the Alexander von Humboldt Foundation in the framework of the Sofja Kovalevskaja Award endowed by the German Federal Ministry of Education and Research. Computational resources were provided by the National Energy Research Scientific Computing Center and the Molecular Foundry, DOE Office of Science User Facilities supported by the Office of Science of the U.S. Department of Energy under Contract No. DE-AC02-05CH11231. Additionally, the authors gratefully acknowledge the computing time granted by the John von Neumann Institute for Computing (NIC) and provided on the supercomputer JURECA92 at the Jülich Supercomputing Center (JSC)[96].

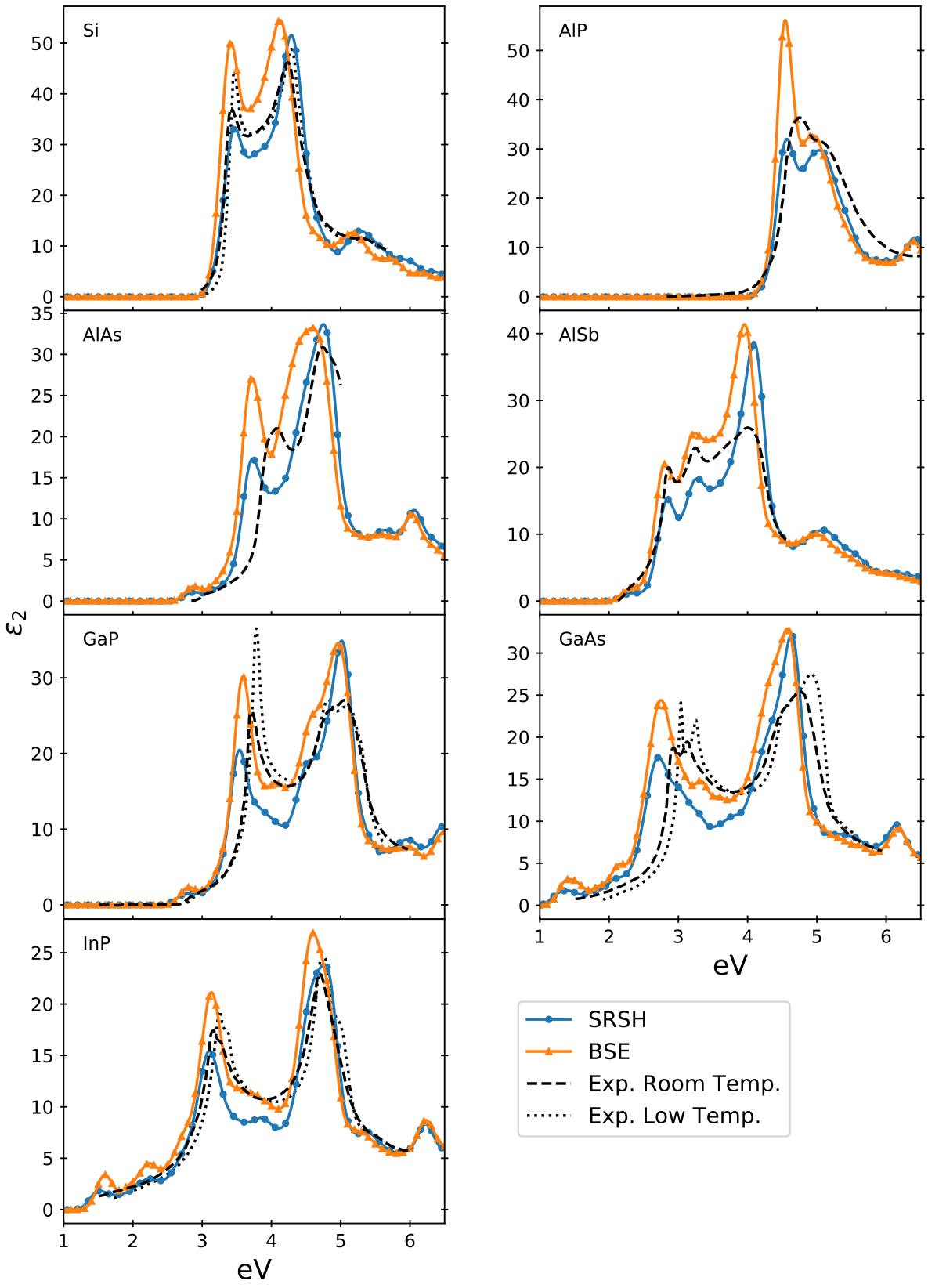

FIG. 3. Optical absorption spectra computed using SRSH with the same parameters as in Fig. 1 (blue circles) and BSE (orange triangles) compared to experiment (dotted lines). All calculations, except for those of Si and AlP, include spin-orbit coupling. Room-temperature experimental data are taken from the following references Si: 90, AlP: 79, AlAs and AlSb: 91, GaP, GaAs, and InP: 92. Low temperature experimental data are taken from Si: 90, GaP: 93, GaAs: 94, and InP: 95

[1] L. Hedin, Phys. Rev. **139**, A796 (1965).
[2] L. Hedin and S. Lundqvist (Academic Press, 1970) pp. 1 – 181.
[3] M. S. Hybertsen and S. G. Louie, Phys. Rev. Lett. **55**, 1418 (1985).
[4] M. S. Hybertsen and S. G. Louie, Phys. Rev. B **34**, 5390 (1986).
[5] F. Aryasetiawan and O. Gunnarsson, Reports on Progress in Physics **61**, 237 (1998).
[6] G. Strinati, Riv. Nuovo Cimento **11**, 1 (1988).
[7] M. Rohlfing and S. G. Louie, Phys. Rev. Lett. **81**, 2312 (1998).
[8] M. Rohlfing and S. G. Louie, Phys. Rev. B **62**, 4927 (2000).
[9] G. Onida, L. Reining, and A. Rubio, Rev. Mod. Phys. **74**, 601 (2002).
[10] E. Runge and E. K. U. Gross, Phys. Rev. Lett. **52**, 997 (1984).
[11] N. T. Maitra, J. Chem. Phys. **144**, 220901 (2016).
[12] C. A. Ullrich, *Time-dependent density-functional theory: concepts and applications* (OUP Oxford, 2011).
[13] K. Burke, J. Chem. Phys. **136**, 150901 (2012).
[14] V. I. Gavrilenko and F. Bechstedt, Phys. Rev. B **55**, 4343 (1997).
[15] Y.-H. Kim and A. Görling, Phys. Rev. Lett. **89**, 096402 (2002).
[16] Z.-h. Yang, F. Sottile, and C. A. Ullrich, Phys. Rev. B **92**, 035202 (2015).
[17] S. Rigamonti, S. Botti, V. Veniard, C. Draxl, L. Reining, and F. Sottile, Phys. Rev. Lett. **114**, 146402 (2015).
[18] Y.-M. Byun and C. A. Ullrich, Phys. Rev. B **95**, 205136 (2017).
[19] A. V. Terentjev, L. A. Constantin, and J. M. Pitarke, Phys. Rev. B **98**, 085123 (2018).
[20] J. P. Perdew and M. Levy, Phys. Rev. Lett. **51**, 1884 (1983).
[21] L. J. Sham and M. Schlüter, Phys. Rev. Lett. **51**, 1888 (1983).
[22] L. Reining, V. Olevano, A. Rubio, and G. Onida, Phys. Rev. Lett. **88**, 066404 (2002).
[23] P. Ghosez, X. Gonze, and R. W. Godby, Phys. Rev. B **56**, 12811 (1997).
[24] S. Botti, F. Sottile, N. Vast, V. Olevano, L. Reining, H.-C. Weissker, A. Rubio, G. Onida, R. Del Sole, and R. W. Godby, Phys. Rev. B **69**, 155112 (2004).
[25] S. Sharma, J. K. Dewhurst, A. Sanna, and E. K. U. Gross, Phys. Rev. Lett. **107**, 186401 (2011).
[26] P. E. Trevisanutto, A. Terentjevs, L. A. Constantin, V. Olevano, and F. D. Sala, Phys. Rev. B **87**, 205143 (2013).
[27] Z. Ning, C.-T. Liang, and Y.-C. Chang, Phys. Rev. B **96**, 085202 (2017).
[28] J. Paier, M. Marsman, and G. Kresse, Phys. Rev. B **78**, 121201 (2008).
[29] S. Tomić, L. Bernasconi, B. G. Searle, and N. M. Harrison, J. Phys. Chem. C **118**, 14478 (2014).
[30] S. Refaely-Abramson, M. Jain, S. Sharifzadeh, J. B. Neaton, and L. Kronik, Phys. Rev. B **92**, 081204 (2015).
[31] A. Seidl, A. Görling, P. Vogl, J. Majewski, and M. Levy, Phys. Rev. B **53**, 3764 (1996).
[32] R. Baer and L. Kronik, Euro. Phys. J. B **91**, 170 (2018).
[33] J. P. Perdew, R. G. Parr, M. Levy, and J. L. Balduz, Phys. Rev. Lett. **49**, 1691 (1982).
[34] M. Levy, J. P. Perdew, and V. Sahni, Phys. Rev. A **30**, 2745 (1984).
[35] L. Kronik, T. Stein, S. Refaely-Abramson, and R. Baer, J. Chem. Theory Comp. **8**, 1515 (2012).
[36] L. Kronik and S. Kümmel, Top. Curr. Chem. **347**, 137 (2014).
[37] S. Kümmel and L. Kronik, Rev. Mod. Phys. **80**, 3 (2008).
[38] J. R. Chelikowsky and M. L. Cohen, Phys. Rev. B **14**, 556 (1976).
[39] X. Zhu and S. G. Louie, Phys. Rev. B **43**, 14142 (1991).
[40] B. D. Malone and M. L. Cohen, J. Phys.: Condens. Matter **25**, 105503 (2013).
[41] J. P. Perdew, K. Burke, and M. Ernzerhof, Phys. Rev. Lett. **77**, 3865 (1996).
[42] P. Giannozzi, S. Baroni, N. Bonini, M. Calandra, R. Car, C. Cavazzoni, D. Ceresoli, G. L. Chiarotti, M. Cococcioni, I. Dabo, A. D. Corso, S. de Gironcoli, S. Fabris, G. Fratesi, R. Gebauer, U. Gerstmann, C. Gougoussis, A. Kokalj, M. Lazzeri, L. Martin-Samos, N. Marzari, F. Mauri, R. Mazzarello, S. Paolini, A. Pasquarello, L. Paulatto, C. Sbraccia, S. Scandolo, G. Sclauzero, A. P. Seitsonen, A. Smogunov, P. Umari, and R. M. Wentzcovitch, J. Phys.: Condens. Matter **21**, 395502 (2009).
[43] P. Giannozzi, O. Andreussi, T. Brumme, O. Bunau, M. B. Nardelli, M. Calandra, R. Car, C. Cavazzoni, D. Ceresoli, M. Cococcioni, N. Colonna, I. Carnimeo, A. D. Corso, S. de Gironcoli, P. Delugas, R. A. D. Jr, A. Ferretti, A. Floris, G. Fratesi, G. Fugallo, R. Gebauer, U. Gerstmann, F. Giustino, T. Gorni, J. Jia, M. Kawamura, H.-Y. Ko, A. Kokalj, E. Küçükbenli, M. Lazzeri, M. Marsili, N. Marzari, F. Mauri, N. L. Nguyen, H.-V. Nguyen, A. O. de-la Roza, L. Paulatto, S. Poncé, D. Rocca, R. Sabatini, B. Santra, M. Schlipf, A. P. Seitsonen, A. Smogunov, I. Timrov, T. Thonhauser, P. Umari, N. Vast, X. Wu, and S. Baroni, J. Phys.: Condens. Matter **29**, 465901 (2017).
[44] D. R. Hamann, Phys. Rev. B **88**, 085117 (2013).
[45] M. L. Tiago, S. Ismail-Beigi, and S. G. Louie, Phys. Rev. B **69**, 125212 (2004).
[46] J. Deslippe, G. Samsonidze, D. A. Strubbe, M. Jain, M. L. Cohen, and S. G. Louie, Comp. Phys. Commun. **183**, 1269 (2012).
[47] F. Aryasetiawan and S. Biermann, Phys. Rev. Lett. **100**, 116402 (2008).
[48] R. Sakuma, C. Friedrich, T. Miyake, S. Blügel, and F. Aryasetiawan, Phys. Rev. B **84**, 085144 (2011).
[49] A. Kutepov, K. Haule, S. Y. Savrasov, and G. Kotliar, Phys. Rev. B **85**, 155129 (2012).
[50] P. Scherpelz, M. Govoni, I. Hamada, and G. Galli, J. Chem. Theory and Comput. **12**, 3523 (2016).
[51] B. A. Barker, J. Deslippe, J. Lischner, M. Jain, O. V. Yazyev, D. A. Strubbe, and S. G. Louie, To Be Submitted (2019).
[52] M. S. Hybertsen and S. G. Louie, Phys. Rev. B **34**, 2920 (1986).
[53] A. Oschlies, R. W. Godby, and R. J. Needs, Phys. Rev. B **51**, 1527 (1995).
[54] R. W. Godby, M. Schlüter, and L. J. Sham, Phys. Rev. B **37**, 10159 (1988).
[55] M. Govoni and G. Galli, J. Chem. Theory and Comput. **11**, 2680 (2015).

[56] H.-V. Nguyen, T. A. Pham, D. Rocca, and G. Galli, Phys. Rev. B **85**, 081101 (2012).
[57] T. A. Pham, H.-V. Nguyen, D. Rocca, and G. Galli, Phys. Rev. B **87**, 155148 (2013).
[58] H. F. Wilson, F. Gygi, and G. Galli, Phys. Rev. B **78**, 113303 (2008).
[59] H. F. Wilson, D. Lu, F. Gygi, and G. Galli, Phys. Rev. B **79**, 245106 (2009).
[60] M. Del Ben, F. H. da Jornada, G. Antonius, T. Rangel, S. G. Louie, J. Deslippe, and A. Canning, Phys. Rev. B **99**, 125128 (2019).
[61] L. Kronik and J. B. Neaton, Annu. Rev. Phys. Chem. **67**, 587 (2016), See section 2.
[62] S. Refaely-Abramson, S. Sharifzadeh, M. Jain, R. Baer, J. B. Neaton, and L. Kronik, Phys. Rev. B **88**, 081204 (2013).
[63] J. H. Skone, M. Govoni, and G. Galli, Phys. Rev. B **93**, 235106 (2016).
[64] G. Miceli, W. Chen, I. Reshetnyak, and A. Pasquarello, Phys. Rev. B **97**, 121112 (2018).
[65] L. Kronik and S. Kümmel, Adv. Mater. **30**, 1706560 (2018).
[66] G. Kresse and J. Furthmüller, Phys. Rev. B **54**, 11169 (1996).
[67] G. Kresse and D. Joubert, Phys. Rev. B **59**, 1758 (1999).
[68] R. W. Nunes and X. Gonze, Phys. Rev. B **63**, 155107 (2001).
[69] I. Souza, J. Íñiguez, and D. Vanderbilt, Phys. Rev. Lett. **89**, 117602 (2002).
[70] J. Heyd, G. E. Scuseria, and M. Ernzerhof, J. Chem. Phys. **118**, 8207 (2003); J. Heyd, *ibid.* **124**, 219906 (2006).
[71] A. A. Mostofi, J. R. Yates, G. Pizzi, Y.-S. Lee, I. Souza, D. Vanderbilt, and N. Marzari, Comput. Phys. Commun. **185**, 2309 (2014).
[72] O. Madelung, *Semiconductors Data Handbook*, 3rd ed. (Springer-Verlag Berlin Heidelberg, 2004).
[73] C. Hilsum, S. Fray, and C. Smith, Solid State Commun. **7**, 1057 (1969).
[74] M. E. Casida, in *Recent Advances in Density Functional Methods part I*, edited by D. P. Chong (World Scientific, Singapore, 1995) Chap. 5, pp. 155–192.
[75] S. Hirata and M. Head-Gordon, Chem. Phys. Lett. **314**, 291 (1999).
[76] M. Welkowsky and R. Braunstein, Phys. Rev. B **5**, 497 (1972).
[77] P. Larson, M. Dvorak, and Z. Wu, Phys. Rev. B **88**, 125205 (2013).
[78] B. Monemar, Phys. Rev. B **8**, 5711 (1973).
[79] S. Hwang, T. Kim, Y. Jung, N. Barange, H. Park, J. Kim, Y. Kang, Y. Kim, S. Shin, J. Song, C.-T. Liang, and Y.-C. Chang, J. Alloy. Compd. **587**, 361 (2014).
[80] J. Klimeš, M. Kaltak, and G. Kresse, Phys. Rev. B **90**, 075125 (2014).
[81] M. van Schilfgaarde, T. Kotani, and S. Faleev, Phys. Rev. Lett. **96**, 226402 (2006).
[82] M. Jain, J. Deslippe, G. Samsonidze, M. L. Cohen, J. R. Chelikowsky, and S. G. Louie, Phys. Rev. B **90**, 115148 (2014).
[83] F. Bruneval and M. A. L. Marques, J. Chem. Theory and Comput. **9**, 324 (2013).
[84] M. Shishkin, M. Marsman, and G. Kresse, Phys. Rev. Lett. **99**, 246403 (2007).
[85] J. H. Skone, M. Govoni, and G. Galli, Phys. Rev. B **89**, 195112 (2014).
[86] R. O. Jones and O. Gunnarsson, Rev. Mod. Phys. **61**, 689 (1989).
[87] M. Rohlfing, P. Krüger, and J. Pollmann, Phys. Rev. B **57**, 6485 (1998).
[88] J. Lischner, G. K. Pálsson, D. Vigil-Fowler, S. Nemsak, J. Avila, M. C. Asensio, C. S. Fadley, and S. G. Louie, Phys. Rev. B **91**, 205113 (2015).
[89] Y. W. Jung, T. H. Ghong, J. S. Byun, Y. D. Kim, H. J. Kim, Y. C. Chang, S. H. Shin, and J. D. Song, Appl. Phys. Lett. **94**, 231913 (2009).
[90] P. Lautenschlager, M. Garriga, L. Vina, and M. Cardona, Phys. Rev. B **36**, 4821 (1987).
[91] C. M. Herzinger, P. G. Snyder, F. G. Celii, Y. Kao, D. Chow, B. Johs, and J. A. Woollam, J. Appl. Phys. **79**, 2663 (1996).
[92] D. E. Aspnes and A. A. Studna, Phys. Rev. B **27**, 985 (1983).
[93] S. Zollner, M. Garriga, J. Kircher, J. Humlíček, M. Cardona, and G. Neuhold, Phys. Rev. B **48**, 7915 (1993).
[94] P. Lautenschlager, M. Garriga, S. Logothetidis, and M. Cardona, Phys. Rev. B **35**, 9174 (1987).
[95] P. Lautenschlager, M. Garriga, and M. Cardona, Phys. Rev. B **36**, 4813 (1987).
[96] D. Krause and P. Thörnig, Journal of large-scale research facilities **2**, 62 (2016).